Desalination and Water Treatment
www.deswater.com

doi: 10.5004/dwt.2017.20562

74 (2017) 163–173
May

N,*N*-Diethylethanolammonium chloride-based DES-functionalized carbon nanotubes for arsenic removal from aqueous solution

Mohamed Khalid AlOmar[a,b], Mohammed Abdulhakim Alsaadi[b,c,d,*], Mustafa Mohammed Aljumaily[c], Shatirah Akib[e], Taha M. Jassam[f], Mohd Ali Hashim[b,g]

[a]*Department of Civil Engineering, University of Malaya, Kuala Lumpur 50603, Malaysia*
[b]*University of Malaya Centre for Ionic Liquids, University of Malaya, Kuala Lumpur 50603, Malaysia, Tel. +60163630693; Fax: +60 3 7967 5311; email: mdsd68j@gmail.com (M.A. Alsaadi)*
[c]*Nanotechnology & Catalysis Research Centre (NANOCAT), IPS Building, University of Malaya, Kuala Lumpur 50603, Malaysia*
[d]*National Chair of Materials Science and Metallurgy, University of Nizwa, Oman*
[e]*School of Science and Engineering, Teesside University, Middlesbrough TS1 3BX, United Kingdom*
[f]*Civil Engineering Department, Faculty of Engineering, Technology and Built Environment, UCSI University, Kuala Lumpur 56000, Malaysia*
[g]*Department of Chemical Engineering, University of Malaya, Kuala Lumpur 50603, Malaysia*

Received 25 September 2016; Accepted 3 February 2017

ABSTRACT

In this study, novel adsorbents for arsenic ions (As^{3+}) were prepared by functionalizing carbon nanotubes (CNTs) with deep eutectic solvents (DESs) based on *N*,*N*-diethyl ethanol ammonium chloride and glycerol. Various characterization techniques were used to investigate the effects of DESs on the surface of CNTs, including Raman, Fourier transform infrared spectroscopy, X-ray powder diffraction, field-emission scanning electron microscopy, energy-dispersive X-ray spectrometer, Brunauer–Emmett–Teller surface area, and zeta potential. Response surface methodology–central composite design experimental design was used to determine the optimum removal conditions, which was found to be at pH 6.0 with adsorbent dosage of 20 mg and contact time of 55 min. The pseudo-second-order kinetics model describes the adsorption of As^{3+}. Moreover, Langmuir isotherm model describes the adsorption isotherm. The maximum adsorption capacity of the novel adsorbent was found to be 17 mg/g.

Keywords: Carbon nanotubes; Arsenic; Adsorption; Deep eutectic solvents

1. Introduction

The presence of arsenic (As) in water, in any oxidation state form, is considered very harmful to humankind and other living orgasms. The As contamination in drinking water has been proposed to cause skin cancer and kidney cancer, lung, bladder, and other internal tumors, vascular diseases, and diabetes [1]. The order of toxicities for arsenic species is as follows: arsenite (As^{3+}) > arsenate (As^{5+}) > monomethyl arsenic acid > dimethyl arsenic acid [2]. Water resources may become contaminated by As either from natural deposits in the earth or through human activities [1,3,4]. The maximum levels of As allowed in drinking water is 10 μg/L according to the World Health Organization (WHO) [5,6]. The contamination of As in water has been reduced using several chemical methods, i.e., coagulation, precipitation, ion exchange, reverse osmosis, and oxidation [7]. However, these techniques have some limitations [8,9]. Therefore, the new alternative or modified technologies can be highly expected. Adsorption can be considered as one of the most effective techniques for removal of As ions, since it is the best in terms of separation for small amount of pollutant from large amounts of solution [10,11]. Various adsorbents, i.e., ferrihydrite [12], activated alumina grains [13],

* Corresponding author.

iron oxide uncoated sand [14], have been used to remove all forms of As ions from solution. These adsorbents still have some problems concerning the low adsorption capacity and difficulty of separating adsorbents from aqueous solutions. Carbon nanotubes (CNTs) have proven to be the excellent adsorbent for many pollutants [15], including cadmium [16], zinc [17], lead [18], and copper [19]. However, the CNTs have many problems like solubility, aggregation, and difficulty of manipulation even though they have many extraordinary physicochemical properties. But CNTs have shown a great affinity for interaction with a variety of different compounds. Enhances CNTs surface with active functional groups to increase the adsorption capacity [20]. However, functionalization with conventional agents can be ineffective or involve chemicals that are harmful for environment. Consequently, the new types of economical and environmentally friendly functionalization agents needed for many applications [21,22]. Including As removal from aqueous solution.

Due to the large amount of interest in the ionic liquids analogues, i.e., deep eutectic solvents (DESs), which were introduced as a cheaper replacement for developed ionic liquids (ILs) by Abbott et al. [23]. They have been used in a large number of applications [24]. Recently, ILs and DESs have been applied in many nanotechnology related fields, such as media for synthesis of nanoparticles, electrolyte for nanostructure sensors, and electrolyte for nanoparticle deposition [25].

In this work, ammonium-based DES composed of *N*,*N*-diethylethanolammonium chloride (DAC), with glycerol (Gly) as hydrogen bond donor, is used as functionalization agent of CNTs. Subsequently, a novel DES/CNTs combination was utilized as an adsorbent of As^{3+} ions from water. The adsorbent was characterized using Raman spectroscopy, X-ray powder diffraction (XRD), Fourier transform infrared (FTIR) spectroscopy, field-emission scanning electron microscope (FESEM), energy-dispersive X-ray spectrometer (EDX), Brunauer–Emmett–Teller (BET), and zeta potential. An optimization study was performed using response surface methodology (RSM) to optimize the removal conditions for As^{3+} adsorption. Moreover, kinetics and isotherm studies were also performed at the potential optimal conditions.

2. Materials and methods

2.1. Chemicals and materials

Multi-wall carbon nanotubes (MWCNTs) with specifications of *D* 6–9 nm × *L* 5 μm > 95% (carbon) were supplied by Sigma-Aldrich (USA). Gly, nitric acid (65%), potassium permanganate, sodium hydroxide pellets, and hydrochloric acid (36.5%–38%) were also supplied by Sigma-Aldrich. DAC and As^{3+} 1,000 mg/L standard solution were supplied by Merck (USA).

2.2. Synthesis of DES

To prepare DESs, DAC was mixed with Gly at a molar ratio of 1:2 using magnetic stirring at 400 rpm and 80°C under atmospheric pressure until the mixture became homogeneous solution. Later, all DESs were stored in well-sealed cups and placed in a desiccator to avoid humidity effects. The details of stability and physical properties of this DES were reported in our previous study [26].

2.3. Oxidation and acidification of MWCNTs

Two types of conventional functionalization were applied to oxidize the pristine MWCNTs (P-CNTs) to prepare them for use in subsequent functionalization steps. The P-CNTs were dried overnight at 100°C. Later, the P-CNTs were sonicated in a solution of $KMnO_4$, in order to produce $KMnO_4$-based CNTs (K-CNTs). The P-CNTs were refluxed with HNO_3 (65%) for 1 h at 140°C to produce HNO_3-based CNTs (N-CNTs). All the functionalized CNTs were washed with distilled water and filtrated with vacuum pump by several times using a polytetrafluoroethylene 0.45 μm membrane.

2.4. Functionalization by DES

7 mL of DAC-based DES was added to 200 mg each of P-CNTs, K-CNTs, and N-CNTs and heated to 65°C with sonication for 3 h to produce (PD-CNTs), (KD-CNTs), and (ND-CNTs), respectively. The mixture was then washed with distilled water by several times and filtered using a 0.45 μm membrane until reaching neutral water. Later, all CNTs samples were dried overnight under vacuum at 100°C and then kept in well-sealed cups in a desiccator. The prepared CNTs samples are listed in Table S1.

2.5. Characterization of functionalized CNTs

High resolution nanosized images were taken along with an EDX using an FESEM (Quanta FEG 450, EDX-OXFORD). The surface modifications and functional groups were identified using FTIR spectroscopy. Raman spectroscopy (Renishaw System 2000 Raman Spectrometer) was used to obtain Raman shift spectra for all adsorbents to evaluate the degree of functionalization. The structure phases were analyzed using an X-ray powder diffraction (XRD), Shimadzu XRD 6000XRD. A fully automated gas sorption system (micromeritics ASAP 2020, TRISTAR II 3020 Kr) was used to study the surface area of the selected samples based on BET method. Furthermore, the surface charge was measured by conducting zeta potential experiments using a Zetasizer (Malvern, UK). The arsenic concentration was measured using inductively coupled plasma with an Optima 7000DV PerkinElmer®.

2.6. Adsorption studies

Primary batch adsorption experiments were carried out in 250 mL flasks. Two sets of stock solution were prepared at pH 2.7 and pH 6.0. Next, 10 mg of P-CNTs, K-CNTs, N-CNTs, PD-CNTs, KD-CNTs, and ND-CNTs were added to 50 mL of As^{3+} stock solution with a concentration of 5 mg/L. The flasks were agitated at 180 rpm for 30 min at room temperature. The adsorbent with the highest removal percentage was chosen for further study.

3. Results and discussion

The results obtained from the primary screening show that KD-CNTs recorded the highest removal percentage at pH

Table 1
Screening study for the removal of As^{3+}

Adsorbent		P-CNTs	K-CNTs	N-CNTs	D-CNTs	KD-CNTs	ND-CNTs
Removal (%)	pH 2.7	0	19.7	0	0	12.29	0
	pH 6.0	0	8.3	0	0	33.99	0

6.0 and this effect increased significantly by increasing pH. The removal percentage of As^{3+} by each adsorbent is listed in Table 1.

3.1. Characterization of the adsorbent

Knowing the zeta potential of nanoparticles is essential to understand the charge of the surface and the long-term stability of the nanoparticle suspension in aqueous solution. Absolute values can be used to quantitatively compare the various stabilities of particle dispersions [27]. It is well known that there are many factors affecting zeta potential measurements, including particle surface charges, pH, conductivity, ion concentration, and temperature [28]. Herein, 2.5 mg of each adsorbent was dispersed in 5 mL of deionized water for zeta potential measurement. The absolute zeta potential value increased from 5.5 to –45.81 mV for P-CNTs and K-CNTs, respectively [29]. High zeta potential value is an indication of the electrokinetic stability of the particles, where those with a low zeta potential tend to coagulate [6]. By addition of oxygen-containing functional groups, such as carbonyl groups and aliphatic carboxylic acids surface, on the surface of CNTs by functionalization with $KMnO_4$ or acid refluxing, the surface electronegativity increased. Consequently, the hydrophilicity of the adsorbent increased, and that is reflected in the adsorption mechanism. Furthermore, functionalization with DAC-based DES decreased the absolute zeta potential value to –37.6 mV. This reduction may be due to the reduction of oxygen functional groups through formation of new groups.

3.1.1. Raman spectroscopy

Raman spectroscopy is a very valuable technique for the characterization of carbon-based nanomaterials. Herein, Raman spectroscopy was used to analyze P-CNTs, K-CNTs, and KD-CNTs. Fig. 1 shows the two major characteristic bands, namely the *G*-band, which usually detected at 1,500–1,600 cm^{-1}, and the *D*-band at 1,350 cm^{-1}. The *D*-band is attributed to the presence of amorphous or disordered carbon in the CNT samples, which is caused by the sp^3-hybridized carbon atoms in the nanotube sidewalls [30,31]. The *G*-band corresponds to the movement in opposite directions of two neighboring carbon atoms in a graphite sheet [32]. The third characteristic band, known for carbon-based nanostructure, is the *D*', which appears as weak shoulder of the *G*-band at higher frequencies and is considered to be a double resonance feature originating from disorder and defects. It is worth mentioning that the *D*' band is undetectable in pure graphite. However, it can be observed in intercalated graphite and MWCNTs [33]. The degree of functionalization can be determined by comparing the intensity of the *D*-band (I_D) to that of the *G*-band (I_G) [34]. In this study, the I_D/I_G ratio increased significantly with $KMnO_4$ functionalization, and after the sequence functionalization step with DAC-based DES. Table 2 lists the values of I_D/I_G for each P-CNTs, K-CNTs, and KD-CNTs.

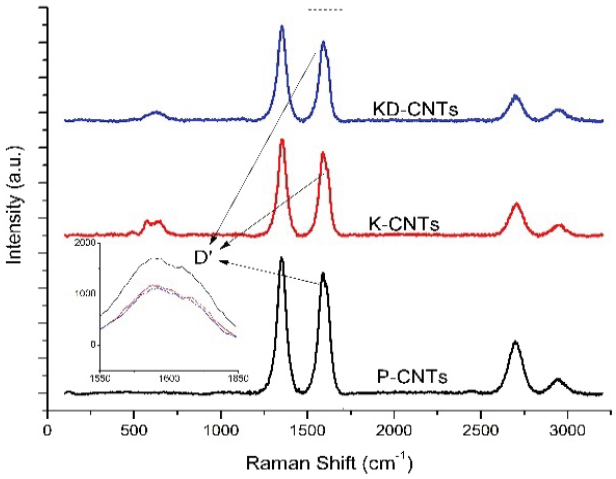

Fig. 1. Raman spectroscopy of each adsorbent.

Table 2
I_D/I_G intensity ratios of each adsorbent

Sample	P-CNTs	K-CNTs	KD-CNTs
I_D/I_G	1.1	1.16	1.2

3.1.2. XRD analysis

Fig. 2 shows the XRD patterns of P-CNTs, K-CNTs, and KD-CNTs. (002) and (001), representing the hexagonal graphite structure and the concentric cylinder structure, respectively, are located at 2θ around 26° and 42° in P-CNTs patterns [35]. The (002) was reduced in the K-CNTs pattern due to the extensive presence of (MnO_2), which was confirmed by the two weak peaks at 2θ around 38° and 65° in K-CNTs pattern [36]. This indicated that deposition of MnO_2 destroys the hexagonal graphite structure of CNTs by wrapping the CNTs into non-stoichiometric, amorphous shapes [37]. The DES functionalization has increased the wrapping around the CNT edges and the main peaks for P-CNT were almost completely disappeared.

3.1.3. FTIR analysis

Fig. 3 shows the FTIR spectrum for P-CNTs, K-CNTs, and KD-CNTs. After functionalization with DAC-based DES, the results demonstrate the detection of N–H stretches

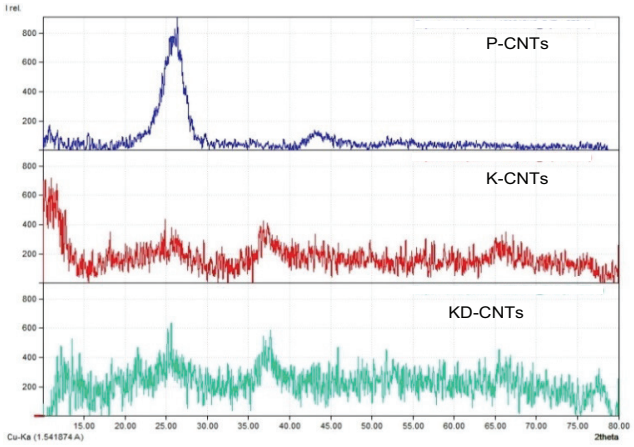

Fig. 2. XRD patterns of P-CNTs, K-CNTs and KKD-CNTs.

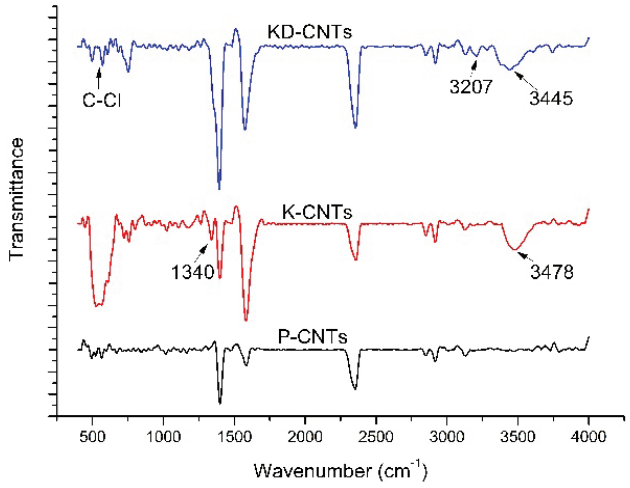

Fig. 3. FTIR spectrum for each adsorbent.

in the range of 3,207 cm^{-1} and stretches for aromatic NH_2 located at 3,445 cm^{-1}, which overlapped with the O–H functional group [38]. In addition, the presence of C–Cl bonds may overlap with other CO groups between 600 and 700 cm^{-1}. Meanwhile the presence of O–H in K-CNTs is located at 3,478 cm^{-1}. The presence of new functional groups after functionalization with DES provides various adsorption sites and increases the adsorption capacity for As^{3+}.

3.1.4. FESEM and EDX

Fig. 4 shows the FESEM images for P-CNTs, K-CNTs, and KD-CNTs. The presence of MnO_2 is not observable in splatted powder or the crystal form, but is embedded within the CNT surface structure, as we can clearly observe in the FESEM images. On the other hand, EDX studies were conducted for KD-CNTs after As^{3+} adsorption. The presence of Mn is observable. In addition, a traceable amount of As^{3+}, Cl^-, O, and N were also observed in the EDX spectrum. Fig. S1 shows the EDX spectrum of KD-CNTs after adsorption. Table S2 listed the elemental percentage on the surface apart from carbon.

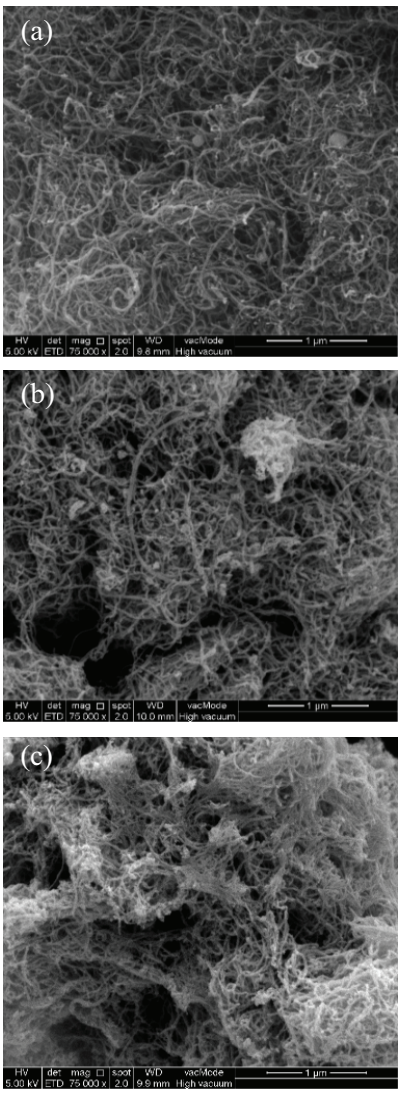

Fig. 4. FESEM images of: (a) P-CNTs, (b) K-CNTs and (c) KD-CNTs.

3.1.5. BET surface area

BET isotherm studies were conducted for P-CNTs, K-CNTs, and KD-CNTs. The results showed that the surface area increased after each functionalization step, due to the functional groups attached to the surface of the adsorbent. Table 3 lists the BET surface areas, total pore volumes, and the average pore diameter. The pore volumes decreased after functionalization by $KMnO_4$, which may be attributed to the presence of MnO_2 partially occupying the space between the CNT surfaces after being embedded within the external surface layers. But the initial pore volume increased again after functionalization with DES, resulting in additional distance gained through charge repulsion from the presence of functional groups with similar electrostatic charges.

3.2. Optimization studies

An estimation of the regression empirical relationship was performed to describe removal percentage and adsorption

Table 3
BET surface area and pore volume and diameter of all adsorbents

Property	P-CNTs	K-CNTs	KD-CNTs
BET surface area (m^2/g)	123.543	158.934	200.583
Total pore volume (cm^3/g)	0.620	0.453	0.648
Average pore diameter (Å)	20.499	114.127	129.411

capacity of As^{3+} using RSM. Central composite design (CCD) was employed using the Design Expert V7.0 software package. The effects and interactions of three parameters were investigated in this study, specifically pH (3–8), contact time (5–55 min), and adsorbent dosage (5–20 mg). The initial concentration and the agitation speed were fixed to 1 mg/L and 180 rpm, respectively. Table S3 lists the design of the experimental runs in terms of the actual parameters, alongside the removal percentage response, and the adsorption capacity response.

Analysis of variance modeling, for As^{3+} removal (%) response and adsorption capacity of KD-CNTs response, indicates significant due to the model *F* values, which were 44.81 and 64.30, respectively. There is only 0.01% and 0.28% chance that the "Model F-Value" this large could occur due to noise for each response, respectively. Eqs. (1) and (2) described the removal of As^{3+} and the adsorption capacity of the KD-CNTs models, respectively. Tables S4 and S5 listed the *p* values, *F* values, and the square mean for both removal and adsorption capacity. Fig. 5 shows the theoretical values plotted vs. the experimental values for the removal percentage and adsorption capacity of KD-CNTs. The R^2 were 0.9782 and 0.9948 for each model, respectively. It is clear that the theoretical values predicted by the models developed in this study were in close agreement with the experimental values, indicating that both models have successfully created correlation between the process variables.

$$As^{3+}\text{removal} = 41.81 + 0.45A + 17.17B + 29.44C + 1.08AB + 2.36AC + 5.81BC \quad (1)$$

$$KD - CNTs\,(\text{Adsorption capacity}) = 0.36 + 0.34A + 0.49B + 0.98C + 0.015AB + 0.37AC - 0.17BC + 0.44A^2 - 0.72C^2 - 0.57A^2C \quad (2)$$

where *A*, *B*, and *C* refer to pH, contact time, and adsorbent dosage, respectively.

Generally, increasing pH of the solution lead to enhance the surface charge of the adsorbent, electrical double layer, and the affinity of metal ion to form seeds of hydroxide which subjected to electrostatic attraction to the surface of the adsorbent. Fig. 6 illustrates the effects of pH on removal percentage, meanwhile, Figs. 7 and 8 show 3D response surfaces to represent the interaction effect between contact time and adsorbent dosage with pH, respectively, on the adsorption capacity. These observations demonstrate that there is a significant effect for pH on adsorption capacity. By fixing the adsorbent dosage to the maximum, the adsorption capacity will increase with increasing pH until reaching the

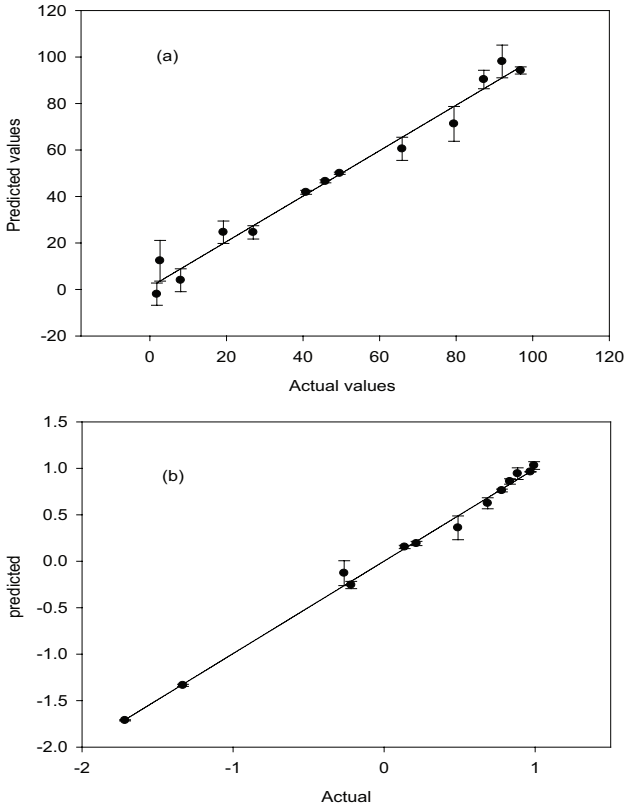

Fig. 5. Theoretical values vs. actual values for: (a) removal response and (b) adsorption capacity response.

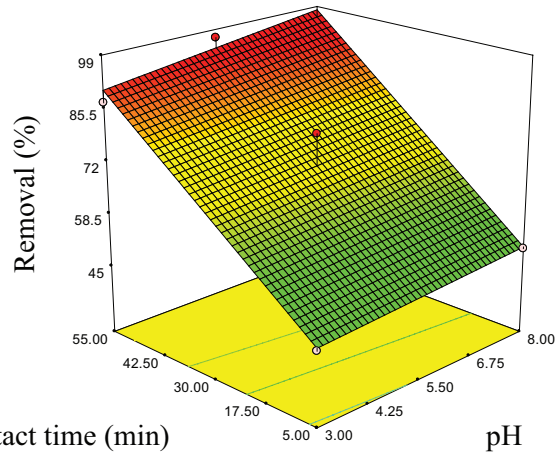

Fig. 6. pH and contact time effect on the removal of As^{3+}.

optimum pH, where it starts to decrease. On the other hand, by fixing the contact time to the maximum, the interaction of adsorbent dosage and pH shows that, at low adsorbent dosage, pH has significant effect on the adsorption capacity. At high adsorbent dosage, the effect of pH decreased and almost vanished.

The optimization functions were set to control the software selection for the optimum adsorption process conditions values, specifically pH, contact time, and adsorbent

dosage. The model variables values, pH, adsorbent dosage, and contact time, were set to be in range. Meanwhile, the two responses, removal percentage of As^{3+} and adsorption capacity of KD-CNTs, were set to the maximum values. Several potential solutions for optimum conditions for As^{3+} adsorption were given by the statistical analysis of CCD. Based on this analysis, the optimum conditions were found to be pH 6.0, adsorbent dosage of 20 mg, and contact time of 55 min, with a desirability of 0.986.

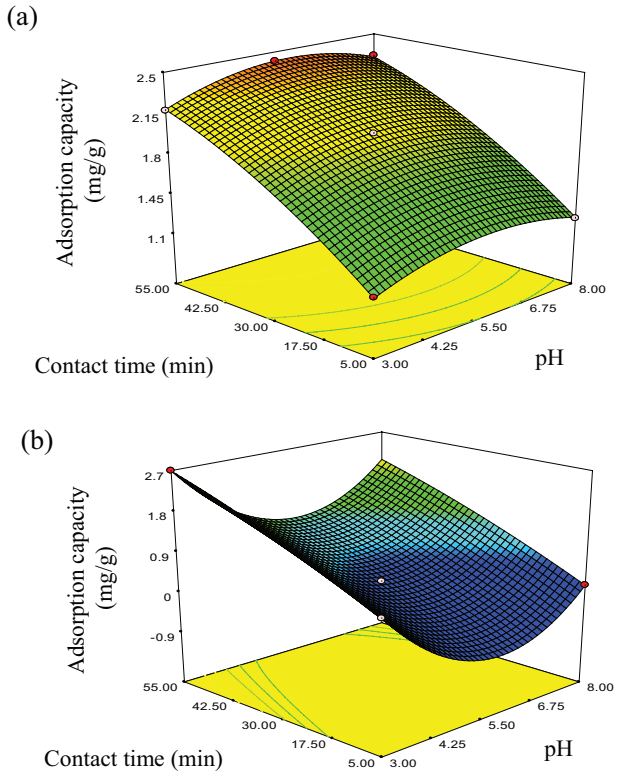

Fig. 7. Effect of pH and contact time on the adsorption capacity of KD-CNTs at: (a) maximum adsorbent dosage and (b) minimum adsorbent dosage.

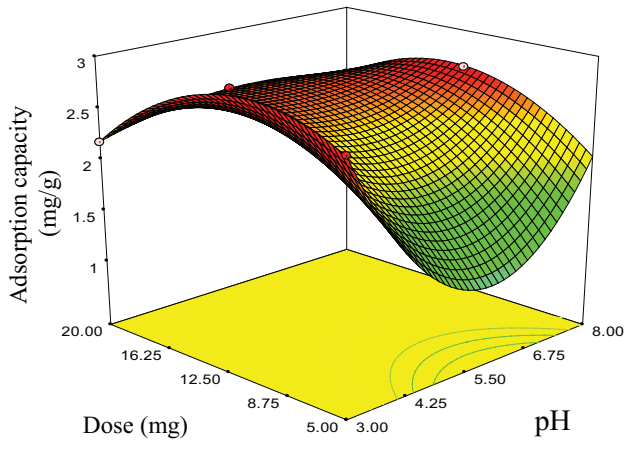

Fig. 8. Effect of pH and adsorbent dosage on the adsorption capacity of KD-CNTs at the optimum contact time.

3.3. Kinetics study

Adsorption kinetics are considered to be one of the most essential characteristics overseeing the rate of ions transferred from the solute to the adsorbent surface, which, furthermore, represents the efficiency of the adsorption process and, hence, determines its potential applications. Pseudo-first-order and pseudo-second-order models were applied to investigate the adsorption kinetics of As^{3+} on the surface of KD-CNTs. The linear form (Eq. (3)) of the pseudo-first-order model described by Lagergren was used to plot the kinetics:

$$\ln(q_e - q_t) = \ln q_e - K_1 t \tag{3}$$

where K_1 and q_e are the slope and intercept calculated by plotting, $\ln(q_e - q_t)$ vs. time (t), respectively. A pseudo-second-order model was also used to study the adsorption kinetics, as described in Eq. (4):

$$\frac{t}{q_t} = \frac{1}{K_2 q_e^2} + \frac{1}{q_e} t \tag{4}$$

where q_e is calculated as 1/(slope) and K_2 is calculated as (slope)^2/intercept. The slope and the intercept were determined from the plot of t/q_t vs. t. In addition, q_e and q_t refer to the adsorption uptake at equilibrium and at time t, respectively.

The conditions applied during kinetic studies were those obtained from the optimization study, i.e., 1 mg/L initial concentration, 20 mg adsorbent dosage, pH 6.0, and agitation speed of 180 rpm. The contact time was 5.5 h to ensure that the reactions reached equilibrium (experimentally 3 h). Fig. 9 shows the plot of pseudo-second-order kinetics model. The values of correlation coefficient R^2 of the data sets were considered as indications of conformity between the experimental data and the corresponding values, as predicted by each model. Herein, the pseudo-second-order rate equation describes the adsorption kinetics of As^{3+} onto KD-CNTs with an R^2 of 0.991. Meanwhile, the pseudo-first-order kinetics model did not fit the adsorption data, since the R^2 was 0.604. The results of the kinetics studies indicate that both the adsorbent and the adsorbate concentrations are involved in the rate determining step, which indicates that the rate-limiting step may be chemisorption. This agreed

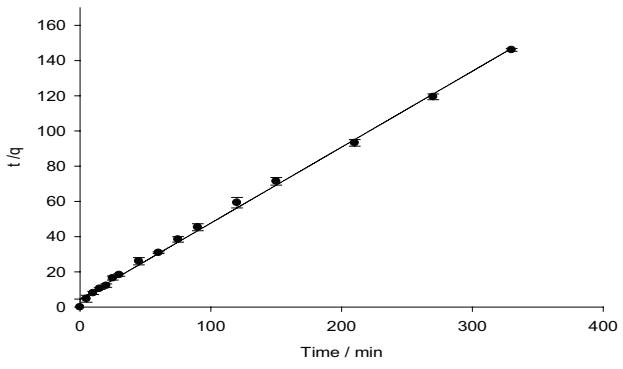

Fig. 9. Plot of pseudo-second-order kinetics model.

Table 4
Isotherm models' parameters and comparison of adsorption capacity of other adsorbents

Adsorption isotherm model		Langmuir			Freundlich			References
Adsorbent	pH	q_m (mg/g)	K_L (L/mg)	R^2	n	K_F (mg/g)	R^2	
KD-CNTs	6	17.085	4.00	0.995	3.29	5.40	0.956	Present work
e-MWCNTs[a]	4	12.175	24.11	0.948	2.77	5.52	0.991	[39]
Fe-MCNTs[b]	8	4.00	1.35	0.996	3.24	2.09	0.987	[6]

[a]e-MWCNTs refer to amino functionalized CNT.
[b]Fe-MCNTs refer to iron oxide modified CNT.

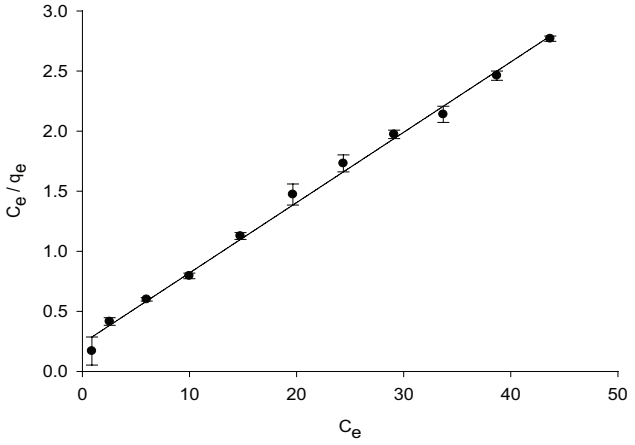

Fig. 10. Linear form of Langmuir isotherm model.

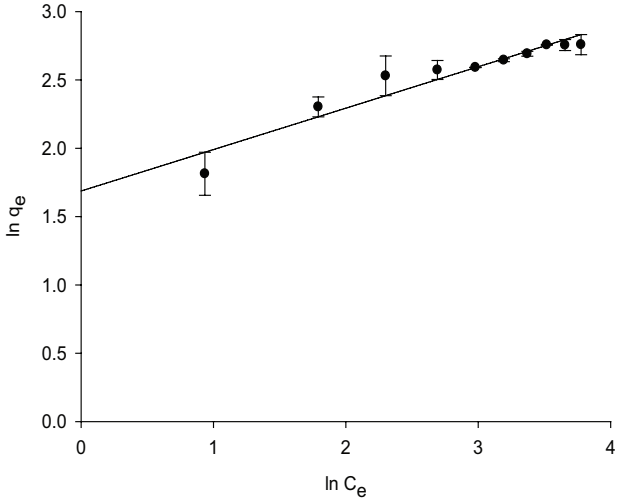

Fig. 11. Linear form of Freundlich isotherm model.

with observations from many CNTs-based adsorbent systems [6,11,39,40].

3.4. Isotherm study

Isotherm studies are essential for any novel adsorbents to investigate the adsorption mechanism, which can be used for future design purposes. Langmuir and Freundlich isotherms adsorption models are the most common isotherm models, which quantify the amount of metal ion adsorbed at equilibrium (q_e) and the solution concentration at equilibrium (C_e) [41]. Herein, 14 As^{3+} initial concentrations (1, 3, 5, 10, 15, 20, 25, 30, 35, 40, 45, 50, 55, and 60 mg/L) were employed to investigate the adsorption isotherm of KD-CNTs. The adsorbent dosage and pH were used at the values indicated in the optimization study.

The Langmuir adsorption isotherm can be described in the linearized form (Eq. (5)) [42]:

$$\frac{C_e}{q_e} = \frac{1}{K_a Q_m} + \left(\frac{1}{Q_m}\right) \times C_e \tag{5}$$

where C_e is the initial equilibrium concentration, and q_e is the amount of metal ions adsorbed on the surface of the adsorbent. K_a and Q_m are the adsorption equilibrium constant and the maximum adsorption capacity, respectively.

The Freundlich model is described by a linearized form (Eq. (6)) [43,44]:

$$\mathrm{In}q_e = \mathrm{In}K_F + \frac{1}{n}\mathrm{In}C_e \tag{6}$$

where q_e is the uptake of the adsorbent and K_F and n are isotherm constants.

The Langmuir isotherm model describes the adsorption of As^{3+} onto the surface of KD-CNTs very well, as the correlation coefficients R^2 were found to be 0.99, which indicates a monolayer coverage of As^{3+} ions on the surface of the KD-CNTs [42]. On the other hand, the corresponding R^2 for the Freundlich isotherm model was 0.95. Figs. 10 and 11 show plots of the Langmuir and Freundlich isotherm models, respectively. Moreover, Table 4 lists the values of the isotherm constants for both models, R^2, the maximum adsorption capacity, and a comparison of the maximum adsorption capacity with previously published results.

4. Conclusion

DAC-based DES was introduced as a functionalization agent of CNTs. Raman spectroscopy, FTIR, XRD, zeta potential, FESEM, and EDX were used to characterize the new adsorbent. The functionalization with DAC–DES introduced new functional groups which enhanced the adsorption of As^{3+}. In addition, the surface area was significantly increased after the functionalization from 123.5 to 200.6 m^2/g. Later, the novel DES–CNTs combination was used as As^{3+} adsorbent.

The removal conditions were optimized using RSM. The optimum removal conditions were found to be at pH 6, adsorption dosage 20 mg, and contact time 55 min. Pseudo-second-order equation describes the adsorption rate order. The maximum adsorption capacity of CNTs functionalized with $KMnO_4$ and DAC–DES was 17.085 mg/g and isotherm data fitted well with the Langmuir isotherm model.

Acknowledgment

The authors express their thanks to the University of Malaya UMRG (RP017B-13AET) for funding this research.

References

[1] Ihsanullah, A. Abbas, A.M. Al-Amer, T. Laoui, M.J. Al-Marri, M.S. Nasser, M. Khraisheh, M.A. Atieh, Heavy metal removal from aqueous solution by advanced carbon nanotubes: critical review of adsorption applications, Sep. Purif. Technol., 157 (2016) 141–161.
[2] J.H. Duffus, "Heavy metals" a meaningless term? (IUPAC Technical Report), Pure Appl. Chem., 74 (2002) 793–807.
[3] B. Black, Arsenic: Answers to Questions Commonly Asked by Drinking Water Professionals, American Water Works Association, USA, 1999.
[4] B.K. Mandal, K.T. Suzuki, Arsenic round the world: a review, Talanta, 58 (2002) 201–235.
[5] P.L. Smedley, D.G. Kinniburgh, United Nations Synthesis Report on Arsenic in Drinking-Water, British Geological Survey, Wallingford, Oxon, UK, 2001, pp. 1–61.
[6] B.S. Tawabini, S.F. Al-Khaldi, M.M. Khaled, M.A. Atieh, Removal of arsenic from water by iron oxide nanoparticles impregnated on carbon nanotubes, J. Environ. Sci. Health, Part A, 46 (2011) 215–223.
[7] A. Al-Mamun, M.A.F.R. Al-Khatib, Z.A. Kadir, Y.M. Ahmed, A. Mohammed, M. Alam, S.A. Muyibi, A.F. Ismail, A. Idris, Optimisation of arsenic adsorption from water by carbon nanofibres grown on powdered activated carbon impregnated with nickel, J. Appl. Sci., 9 (2009) 3180–3183.
[8] K.B. Payne, T.M. Abdel-Fattah, Adsorption of arsenate and arsenite by iron-treated activated carbon and zeolites: effects of ph, temperature, and ionic strength, J. Environ. Sci. Health, Part A, 40 (2005) 723–749.
[9] T. Tuutijärvi, J. Lu, M. Sillanpää, G. Chen, As(V) adsorption on maghemite nanoparticles, J. Hazard. Mater., 166 (2009) 1415–1420.
[10] I. Ali, New generation adsorbents for water treatment, Chem. Rev., 112 (2012) 5073–5091.
[11] G. Sheng, Y. Li, X. Yang, X. Ren, S. Yang, J. Hu, X. Wang, Efficient removal of arsenate by versatile magnetic graphene oxide composites, RSC Adv., 2 (2012) 12400–12407.
[12] K.P. Raven, A. Jain, R.H. Loeppert, Arsenite and arsenate adsorption on ferrihydrite: kinetics, equilibrium, and adsorption envelopes, Environ. Sci. Technol., 32 (1998) 344–349.
[13] T.-F. Lin, J.-K. Wu, Adsorption of arsenite and arsenate within activated alumina grains: equilibrium and kinetics, Water Res., 35 (2001) 2049–2057.
[14] V.K. Gupta, V.K. Saini, N. Jain, Adsorption of As(III) from aqueous solutions by iron oxide-coated sand, J. Colloid Interface Sci., 288 (2005) 55–60.
[15] R.K. Ibrahim, M. Hayyan, M.A. AlSaadi, A. Hayyan, S. Ibrahim, Environmental application of nanotechnology: air, soil, and water, Environ. Sci. Pollut. Res., 23 (2016) 1–35. doi: 10.1007/s11356-016-6457-z.
[16] N.M. Mubarak, J.N. Sahu, E.C. Abdullah, N.S. Jayakumar, P. Ganesan, Microwave assisted multiwall carbon nanotubes enhancing Cd(II) adsorption capacity in aqueous media, J. Ind. Eng. Chem., 24 (2015) 24–33.
[17] R.K. Thines, N.M. Mubarak, M. Ruthiraan, E.C. Abdullah, J.N. Sahu, N.S. Jayakumara, P. Ganesan, N.R. Sajuni, Adsorption isotherm and thermodynamics studies of Zn(II) on functionalized and non-functionalized carbon nanotubes, Adv. Sci. Eng. Med., 6 (2014) 974–984.
[18] N.M. Mubarak, J.N. Sahu, E.C. Abdullah, N.S. Jayakumar, Rapid adsorption of toxic Pb(II) ions from aqueous solution using multiwall carbon nanotubes synthesized by microwave chemical vapor deposition technique, J. Environ. Sci., 45 (2016) 143–155.
[19] N.M. Mubarak, J.N. Sahu, E.C. Abdullah, N.S. Jayakumar, P. Ganesan, Novel microwave-assisted multiwall carbon nanotubes enhancing Cu (II) adsorption capacity in water, J. Taiwan Inst. Chem. Eng., 53 (2015) 140–152.
[20] M.K. AlOmar, M.A. Alsaadi, M. Hayyan, S. Akib, R.K. Ibrahim, M.A. Hashim, Lead removal from water by choline chloride based deep eutectic solvents functionalized carbon nanotubes, J. Mol. Liq., 222 (2016) 883–894.
[21] M.T. Martínez, M.A. Callejas, A.M. Benito, M. Cochet, T. Seeger, A. Ansón, J. Schreiber, C. Gordon, C. Marhic, O. Chauvet, W.K. Maser, Modifications of single-wall carbon nanotubes upon oxidative purification treatments, Nanotechnology, 14 (2003) 691.
[22] M. Hayyan, A. Abo-Hamad, M. AlSaadi, M. Hashim, Functionalization of graphene using deep eutectic solvents, Nanoscale Res. Lett., 10 (2015) 1–26.
[23] A.P. Abbott, G. Capper, D.L. Davies, R.K. Rasheed, V. Tambyrajah, Novel solvent properties of choline chloride/urea mixtures, Chem. Commun., 7 (2003) 70–71. doi: 10.1039/B210714G(2003).
[24] E.L. Smith, A.P. Abbott, K.S. Ryder, Deep eutectic solvents (DESs) and their applications, Chem. Rev., 114 (2014) 11060–11082.
[25] A. Abo-Hamad, M. Hayyan, M.A. AlSaadi, M.A. Hashim, Potential applications of deep eutectic solvents in nanotechnology, Chem. Eng. J., 273 (2015) 551–567.
[26] M.K. AlOmar, M. Hayyan, M.A. Alsaadi, S. Akib, A. Hayyan, M.A. Hashim, Glycerol-based deep eutectic solvents: physical properties, J. Mol. Liq., 215 (2016) 98–103.
[27] Z. Sun, V. Nicolosi, D. Rickard, S.D. Bergin, D. Aherne, J.N. Coleman, Quantitative evaluation of surfactant-stabilized single-walled carbon nanotubes: dispersion quality and its correlation with zeta potential, J. Phys. Chem. C, 112 (2008) 10692–10699.
[28] G.S. Simate, S.E. Iyuke, S. Ndlovu, M. Heydenrych, The heterogeneous coagulation and flocculation of brewery wastewater using carbon nanotubes, Water Res., 46 (2012) 1185–1197.
[29] M.K. AlOmar, M.A. Alsaadi, M. Hayyan, S. Akib, M.A. Hashim, Functionalization of CNTs surface with phosphonuim based deep eutectic solvents for arsenic removal from water, Appl. Surf. Sci., 389 (2016) 216–226.
[30] J.L. Bahr, J. Yang, D.V. Kosynkin, M.J. Bronikowski, R.E. Smalley, J.M. Tour, Functionalization of carbon nanotubes by electrochemical reduction of aryl diazonium salts: a bucky paper electrode, J. Am. Chem. Soc., 123 (2001) 6536–6542.
[31] V. Datsyuk, M. Kalyva, K. Papagelis, J. Parthenios, D. Tasis, A. Siokou, I. Kallitsis, C. Galiotis, Chemical oxidation of multiwalled carbon nanotubes, Carbon, 46 (2008) 833–840.
[32] H. Hiura, T.W. Ebbesen, K. Tanigaki, H. Takahashi, Raman studies of carbon nanotubes, Chem. Phys. Lett., 202 (1993) 509–512.
[33] C.S. Kumar, Raman Spectroscopy for Nanomaterials Characterization, Springer Science & Business Media, USA, 2012.
[34] T.J. Aitchison, M. Ginic-Markovic, J.G. Matisons, G.P. Simon, P.M. Fredericks, Purification, cutting, and sidewall functionalization of multiwalled carbon nanotubes using potassium permanganate solutions, J. Phys. Chem. C, 111 (2007) 2440–2446.
[35] D. Zhang, L. Shi, J. Fang, X. Li, K. Dai, Preparation and modification of carbon nanotubes, Mater. Lett., 59 (2005) 4044–4047.
[36] M.K. AlOmar, M.A. Alsaadi, M. Hayyan, S. Akib, M. Ibrahim, M.A. Hashim, Allyl triphenyl phosphonium bromide based DES-functionalized carbon nanotubes for the removal of mercury from water, Chemosphere, 167 (2017) 44–52.
[37] S.-G. Wang, W.-X. Gong, X.-W. Liu, Y.-W. Yao, B.-Y. Gao, Q.-Y. Yue, Removal of lead(II) from aqueous solution by adsorption onto manganese oxide-coated carbon nanotubes, Sep. Purif. Technol., 58 (2007) 17–23.

[38] B.C. Smith, Infrared Spectral Interpretation: A Systematic Approach, CRC Press, USA, 1998.
[39] Z.S. Veličković, A.D. Marinković, Z.J. Bajić, J.M. Marković, A.A. Perić-Grujić, P.S. Uskokovic, M.D. Ristic, Oxidized and ethylenediamine-functionalized multi-walled carbon nanotubes for the separation of low concentration arsenate from water, Sep. Purif. Technol., 48 (2013) 2047–2058.
[40] J. Gong, J. Feng, J. Liu, Z. Jiang, X. Chen, E. Mijowska, X. Wen, T. Tang, Catalytic carbonization of polypropylene into cup-stacked carbon nanotubes with high performances in adsorption of heavy metallic ions and organic dyes, Chem. Eng. J., 248 (2014) 27–40.
[41] X. Liu, W. Wei, X. Zeng, B. Tang, X. Liu, H. Xiang, Copper adsorption kinetics onto pseudomonas aeruginosa immobilized multiwalled carbon nanotubes in an aqueous solution, Anal. Lett., 42 (2009) 425–439.
[42] I. Langmuir, The constitution and fundamental properties of solids and liquids. Part I. Solids, J. Am. Chem. Soc., 38 (1916) 2221–2295.
[43] A. Al Mamun, Y.M. Ahmed, M.a.F.R. AlKhatib, A.T. Jameel, M.A.H.A.R. AlSaadi, Lead sorption by carbon nanofibers grown on powdered activated carbon — kinetics and equilibrium, Nano, 10 (2015) 1550017.
[44] H. Freundlich, H.S. Hatfield, Colloid and capillary chemistry, Methuen and Co. Ltd., London, 1926.

Supplementary information

Table S1
List of CNT-based adsorbents with abbreviations

CNTs based	P-CNTs	K-CNTs	N-CNTs
DES			
D	PD-CNTs	KD-CNTs	ND-CNTs

Note: D refers to DAC-based DES, P refers to pristine, K refers to $KMnO_4$, and N refers to HNO_3.

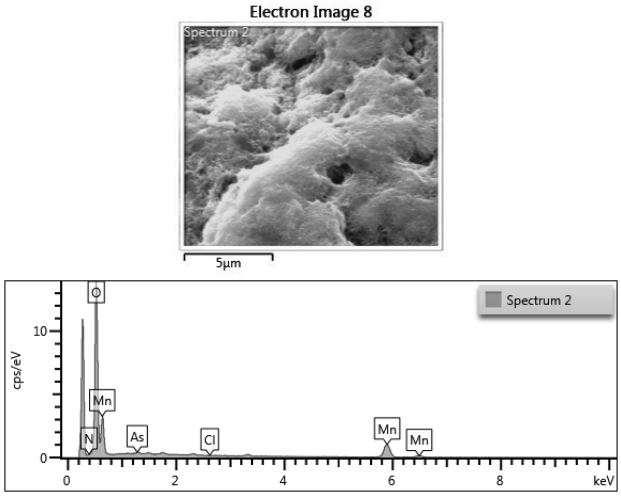

Fig. S1. EDX spectrum of KD-CNTs after the adsorption of As^{3+}.

Table S2
Weight percentage for all elements on the surface of KD-CNTs apart from carbon

Element	Line type	Apparent concentration	*k* Ratio	Wt%	Wt% Sigma	Atomic %
N	K series	0.37	0.00066	0.97	0.22	2.13
O	K series	7.85	0.02642	31.29	0.60	60.11
Cl	K series	0.00	0.00002	0.02	0.13	0.02
Mn	K series	5.55	0.05547	66.82	0.66	37.38
As	L series	0.09	0.00048	0.90	0.25	0.37
Total				100.00		100.00

Table S3
List of design of experimental runs and responses for KD-CNTs

Run	pH	Contact time	Dosage	Response (1) Removal (%)	Response (2) Uptake capacity
1	8	5	20	49.56	1.239
2	8	5	5	1.8	0.18
3	3	55	20	87.24	2.181
4	3	5	5	8.04	0.804
5	5.5	5	12.5	19.2	0.768
6	3	5	20	45.84	1.146
7	5.5	30	20	79.44	1.986
8	5.5	30	12.5	40.8	1.632
9	8	55	20	92.04	2.301
10	5.5	55	20	96.84	2.421
11	5.5	30	5	2.64	0.264
12	3	55	5	27	2.7
13	8	55	12.5	65.88	2.6352

Table S4
2FI model analysis of variance (ANOVA) for As^{3+} removal (%) on KD-CNTs

Source	Sum of squares	df	Mean square	*F* value	*p* Value Prob > *F*	Status
Model	13,974.59	6	2,329.099	44.81419	0.0001	Significant
A	1.46585	1	1.46585	0.028204	0.8721	Not significant
B	2,503.438	1	2,503.438	48.16866	0.0004	Significant
C	7,258.822	1	7,258.822	139.667	<0.0001	Significant
AB	8.550759	1	8.550759	0.164525	0.6991	Not significant
AC	32.4325	1	32.4325	0.624034	0.4596	Not significant
BC	217.0436	1	217.0436	4.176136	0.0870	Not significant

Note: R^2 0.9782, Adj. R^2 0.9563, Pred. R^2 0.8417, and Adeq. precision 18.919.
A: pH, *B*: adsorbent dosage, and *C*: contact time.

Table S5
Reduced cubic model analysis of variance (ANOVA) for As^{3+} adsorption capacity onto KD-CNTs

Source	Sum of squares	df	Mean square	*F* value	*p* Value Prob > *F*	Status
Model	9.104728	9	1.011636	64.30141	0.0028	Significant
A	0.730939	1	0.730939	46.45978	0.0065	Significant
B	1.973772	1	1.973772	125.4565	0.0015	Significant
C	2.477917	1	2.477917	157.5008	0.0011	Significant
AB	0.001415	1	0.001415	0.089945	0.7838	Not significant
AC	0.742896	1	0.742896	47.21981	0.0063	Significant
BC	0.156196	1	0.156196	9.928121	0.0512	Significant
A^2	0.485909	1	0.485909	30.88525	0.0115	Significant
C^2	0.799777	1	0.799777	50.83524	0.0057	Significant
A^2C	0.580801	1	0.580801	36.91676	0.0090	Significant

Note: R^2 0.9948, Adj. R^2 0.9794, Pred. R^2 0.9220, Adeq. precision 24.926.
A: pH, *B*: adsorbent dosage, and *C*: contact time.